Batteries & Supercaps

Research Article
doi.org/10.1002/batt.202200434

Chemistry Europe
European Chemical Societies Publishing

www.batteries-supercaps.org

Special Collection

β-Ketoenamine-Linked Covalent Organic Framework with Co Intercalation: Improved Lithium-Storage Properties and Mechanism for High-Performance Lithium-Organic Batteries

Han Wang[+],[a] Wentao Zou[+],[a] Chao Liu,[a] Yi Sun,[a] Yi Xu,[a] Weiwei Sun,*[a] and Yong Wang*[a]

As a new kind of crystalline porous polymers, covalent organic frameworks (COFs) exhibit great potential as electrode materials for rechargeable metal-ion batteries due to their stable and adjustable structure, high porosity and abundant electrochemical active centers. In this paper, facile one-step synthesis process is proposed to obtain the cobalt ion intercalated two-dimensional β-ketoenamine-linked COF (Co–DAAQ–TFP-COF, denoted as Co-COF). The intercalation of Co ion in adjacent two layered structure of COF via coordination effects can activate the Li^+ storage ability of aromatic ring in the original COF, greatly improve the utilization of redox active sites, shorten the migration length of electrons and ions, and promote fast lithium reaction kinetics. Adopted as the anode for lithium-ion batteries, substantial improvement on the reversible capacity and cycling performance can be achieved for the obtained Co intercalated COF electrode (780 mAh g^{-1} after 200 cycles at 100 mA g^{-1}) compared to original COF electrode (120 mAh g^{-1} under the same condition). The two-dimensional COF materials with morphology justification and/or performance improvement via metal ion intercalation would promote the application of COF related electrodes for other energy-storage fields.

Introduction

With the energy shortage and power consumption, exploring new energy production and low-cost energy storage technology has become the focus in this field. As the power source of portable electronic products, electric vehicles and smart grid, lithium-ion battery (LIB) has been widely used because of its high specific energy density, high output voltage, long cycle life and good safety performance.[1–4] However, the performance of lithium-ion battery is highly dependent on the efficiency of the anode. The exploration and development of high-performance and sustainable green anode materials is very important for the application of lithium-ion batteries.[5] At present, the most widely-explored anode materials for lithium-ion batteries focus on the inorganic materials, including the Sn/Si-based materials, carbonaceous materials, metal oxides/sulfides and their composites, and so on. The inherent disadvantages, such as the limited resources and environmental unfriendliness, significantly limit the broad practical application of inorganic electrode materials.[6,7]

Organic electrode materials have become attractive alternative electrode materials and have been widely adopted in the field of lithium-ion batteries recently.[8–11] Especially the metal-organic framework (MOFs)[12,13] and covalent organic framework (COFs)[14,15] have attracted more attentions, due to their advantages of flexible design, low cost and environmental-friendliness. Covalent organic framework (COF), as a kind of crystalline polymers assembled by covalent bonds through reversible reactions, exhibits high porosity with uniform nano-porous structure. The morphology and the porous structure with pore size of COF can be adjusted by selecting the assembled monomers with desired length and geometry at the molecular level. Recently, many reports on the application of COF in photocatalysis,[16,17] CO_2 adsorption,[18] electrochemical energy storage[19–25] and other fields[26,27] have been reported. It is worth noting that the π-electron delocalization of π-orbital overlap and the maximum energy induced from the van der Waals interaction result in the high specific surface area and high porosity of COF materials, leading to more accessible active sites for energy-storage reactions. Thus, the COF materials have been considered as the excellent candidates for constructing organic electrodes for lithium-ion batteries (LIBs).[28–31] For example, Zhao and his colleagues designed a covalent organic framework (Tp–Azo-COF) materials with double active reaction sites of N=N and C=O groups, extended conjugated structure, large specific surface area and accessible Li^+ transport channels with applying as the anode for LIBs. After 3000 cycles, such COF based anode provides a specific capacity of ~306 mAh g^{-1} under the current density of 1000 mA g^{-1}.[32] However, when most COF and related materials are adopted as electrodes for LIBs, the achievable capacity is extremely limited by the inadequate exposure of redox sites,[33,34] in which more lithium-ion reaction sites are still

[a] H. Wang,[+] W. Zou,[+] C. Liu, Y. Sun, Dr. Y. Xu, Dr. W. Sun, Prof. Y. Wang
School of Environmental and Chemical Engineering, Shanghai University, 99 Shangda Road, Shanghai, 200444, People's Republic of China
E-mail: vivisun@shu.edu.cn
yongwang@shu.edu.cn

[+] These authors contributed equally to this work.

Supporting information for this article is available on the WWW under https://doi.org/10.1002/batt.202200434

Special Collection An invited contribution to a Special Collection on Organic Batteries

Research Article
doi.org/10.1002/batt.202200434
Chemistry Europe
European Chemical Societies Publishing

needed to be activated during the long repetitive charge-discharge process.[35,36] Therefore, how to design and synthesize COF materials with abundant activated redox sites and fast electron transport pathways have become the hot issues for the application of COF electrodes for LIBs.[37–39] For example, Haldar and his coworkers report the chemically stripped anthracyl COF with multiple carbonyl groups interacting with Li^+ ions. It results in the storage of 30 Li^+ per unit (compared to each C_6–Li) of COF structure and the increased specific capacity (200–790 mAh g^{-1}@100 mA g^{-1}, four times of original COF). In addition, more efforts have been put into the improvement on the inherent limitation of poor conductivity for COF materials,[30,34,40] the solution of metal modification on COF structure can achieve the improved conductivity along with the resultant fast kinetics of lithium ion migration.[41–44] Although many metal modified COF composites have been widely used in the field of catalysis,[42,44,45] there are rare reports on the metal modified COF composites as the organic electrode material for lithium-ion batteries.

Herein, a transition metal ion (Co^{2+}) intercalated β-ketoenamine-linked COF (DT-COF) composite (Co–DAAQ–TFP-COF, denoted as Co-COF for short) was prepared through a facile one-step method by introducing Co salts into the synthetic process of DT-COF. Based on the first principles density functional theory (DFT) calculations, the coordination mode of Co ions and the lithium-ion transfer ability of Co-COF have been demonstrated. When adopted as the anode for lithium-ion batteries, the modified Co-COF intercalation electrode delivered enhanced electrical conductivity and activated Li ion storage on aromatic rings and –NH– groups of COF structure with fast reaction kinetics, leading to the improved lithium-storage performances with high reversible capacity of 780 mAh g^{-1} after 200 cycles at 100 mA g^{-1}. Besides, the lithium-reaction mechanism on the Co-COF electrode has also been explored based on *in-situ*/*ex-situ* experimental observation along with DFT calculation.

Results and Discussion

The synthesis process of pristine DT-COF was conducted according to the previous reports,[46] as illuminated in Figure S1. Based on the amine-based reaction between 2,6-diaminoanthraquinone (DAAQ) and 1,3,5-triformyl-2,4,6-trihydroxybenzene (TFP), the product of two-dimensional DT-COF can be obtained. With the addition of cobalt acetate tetrahydrate in the solvothermal synthesized process of DT-COF in the mixed solvent of 1,4-dioxane, mesitylene and 6 M acetic acid, the Co-COF composite with Co ion intercalated COF can be prepared (Figure 1a). It is indicated that the coordination effects between Co metal ions and the coordination-active O sites from the COF structure can lead to the effective combination between each other in Co-COF. Benefited from the metal centers intercalation, the activated lithium-reaction functional groups in DT-COF structure and improved conductivity can be achieved, when applied as the anode material of lithium-ion battery.

The morphological characteristics of DT-COF and Co-COF composite were explored by Scanning Electron Microscope (SEM) and Transmission Electron Microscope (TEM) (Figure 1b–e). For original DT-COF, the stacked nanotube morphology with the tube diameter of ~38 nm can be observed. After Co ion intercalation, the nanotube morphology of COF has been partially destroyed, and rough surface with larger diameter (~60 nm) can be detected for the Co-COF composite, which is probably originated from the expanding layered distance of 2D DT-COF structure with the intercalated Co ions in adjacent layers. In addition, the element mapping image (Figure 1f–j) shows the uniform distribution of the four elements C, N, O and Co in the Co-COF sample, indicating the successful synthesis of DT-COF and the existence of Co ions. It is worth noting that the partially destroyed nanotube structure with Co intercalation can provide more exposed active sites and/or defects for further applications of Co-COF composite.[47]

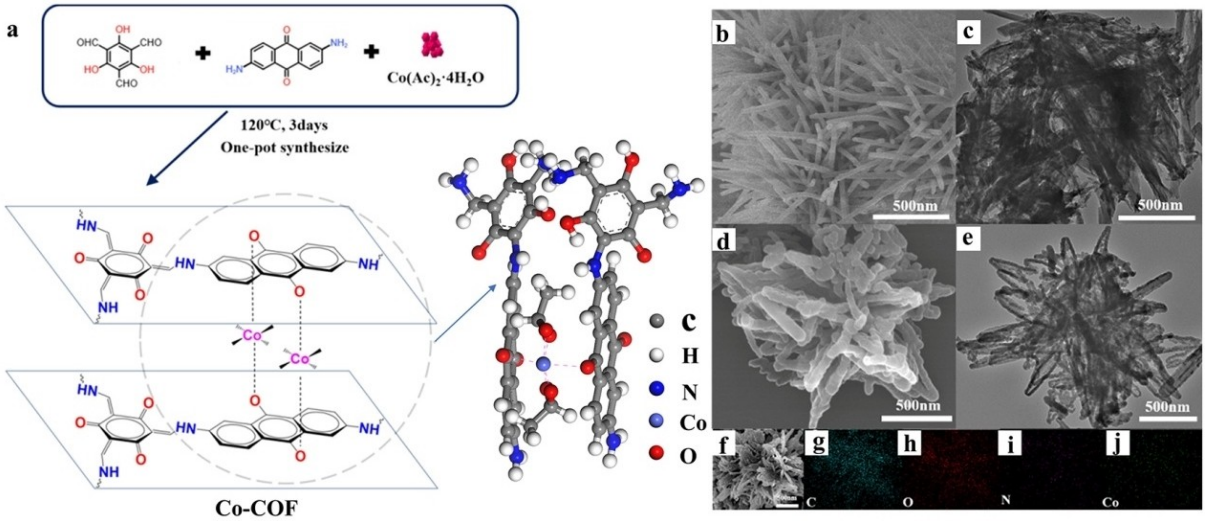

Figure 1. a) Schematic illumination of the synthesis process and the structure of the as-prepared Co-COF composite. b) SEM and c) TEM images of DT-COF. d) SEM and e) TEM images of Co-COF. f–j) Elemental mapping images of Co-COF.

Research Article
doi.org/10.1002/batt.202200434

The Fourier transform infrared spectrum (FT-IR) and powder X-ray diffraction (XRD) have been conducted on the Co-COF and DT-COF samples to illuminate their structure and crystallinity (Figure 2). The characteristic peaks of 1581 and 1619 cm^{-1} in the FT-IR spectrum of DT-COF can be assigned to its C=C and C=O functional groups, and the newly-appeared peak of 1265 cm^{-1} (compared to the reactants of DAAQ and TFP) assigned to the C–N groups, indicating the successful fabrication of DT-COF based on the amine-based reaction between DAAQ and TFP.[48,49] It can also be confirmed by the solid-state ^{13}C CP-MAS NMR spectra of COF (Figure S2), in which the chemical shift at ~150 ppm indicates the formation of =C–NH– units.[50] After the intercalation of Co ions, the FT-IR spectrum of Co-COF delivers slightly difference from that of DT-COF. The characteristic peaks for C=C and C=O units can both be detected, indicating the maintained DT-COF structure in Co-COF with Co. It is worth noting that the characteristic peaks of 1330 and 1657 cm^{-1} in the FT-IR spectrum of Co-COF can be attributed to the carboxyl groups from acetate unit originating from the addition of the $Co(Ac)_2$.[51] Based on the XRD results in Figure 2b, the diffraction peaks at 3.37°, 6.06°, 6.70°, 10.01°, 13.80°, 24.20° and 28.08° correspond to the lattice planes of (100), (110), (220), (200), (210), (202) and (001) for DT-COF, respectively, which is in accordance with previously literatures.[46] Comparatively, the strong characteristic peak at 3.37° can be detected without change in the XRD pattern of Co-COF, while the slight change for other peaks can be ascribed to the reduced crystallinity and changed lattice planes with enlarged layered distance. N_2 adsorption/desorption analysis was conducted to characterize the porosity and specific surface area of DT-COF and Co-COF, as indicated in Figure S3. The specific surface areas of DT-COF and Co-COF can be calculated to be 947.5 and 179.2 $m^2 g^{-1}$, respectively. The decrease of the specific surface area is probably originated from the occupation of pores in COF structure by the intercalated Co ions.[51] In addition, the pore size contribution of Co-COF (2.5–6.6 nm) is similar with that of DT-COF (2.5–8.5 nm), confirming the maintained porous structure for Co-COF, which is beneficial for the lithium-ion transportation during lithium-storage application.

In order to further explore the existence mode of Co element in Co-COF, the X-ray Photoelectron Spectroscopy (XPS) was conducted. As shown in XPS spectrum of Co-COF (Figure 2c), the characteristic peaks for C, N, O and Co elements can be detected. Two peaks at 780.4 and 796.4 eV in Co 2p high resolution XPS spectrum (Figure 2d) with their satellite peaks of 801.8 and 783.9 eV can be assigned to Co $2p_{3/2}$ and Co $2p_{1/2}$ of Co^{2+}, respectively. It gives evidence to the existence of Co ions with the covalent state of II. However, the binding energy (784.3 eV) of Co $2p_{3/2}$ in Co-COF exhibits a negative shift of 3.9 eV compared with that (784.3 eV) of Co $2p_{3/2}$ in $Co(OAc)_2$, indicating the coordination interaction on the Co centers in the Co-COF structure.[51] It is worth noting that the structure of DT-COF is reciprocal by keto-form and enol-form, in which the keto-form structure is dominant,[46] as displayed in Figure S1. Besides the peaks at 531.2 and 532.8 eV assigned to the C=O and C–O groups, which can also be observed in the O 1s spectrum of DT-COF (Figure S4), the peak at 530.8 eV assigned

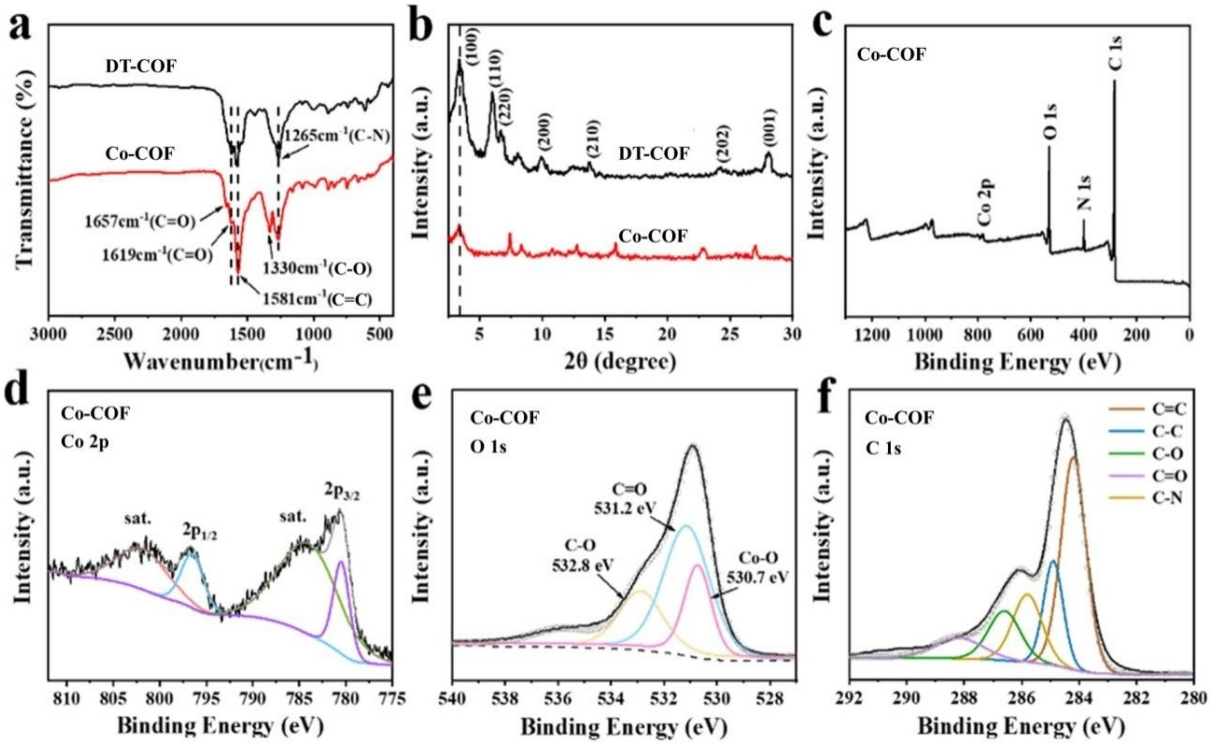

Figure 2. a) FT-IR spectra of Co-COF and DT-COF. b) XRD patterns of Co-COF and DT-COF. XPS spectra of Co-COF: c) the survey spectrum, d) Co 2p spectrum, e) O 1s spectrum, and f) C 1s spectrum.

Research Article
doi.org/10.1002/batt.202200434
Chemistry Europe
European Chemical Societies Publishing

to the Co–O units can also be detected in the O 1s spectrum of Co-COF (Figure 2e). It also proves the successful combination of Co and O in the structure of Co-COF. As indicated in Figure 2f, the high-resolution C 1s XPS spectrum of Co-COF exhibits five peaks at 288.2, 286.6, 285.8, 284.9 and 284.2 eV, corresponding to C=O, C–O, C–N, C–C and C=C groups, respectively.[52]

It indicates that the Co intercalation in the Co-COF composite delivers coordination effects with O atoms from the keto- groups of COF structure based on the XRD and XPS results. In order to demonstrate the detailed coordination mode of Co centers in the Co-COF structure, the first principles density functional theory (DFT) calculation with the Perdew-Burke-Ernzerhof (PBE) functional based on generalized gradient approximation (GGA) has been adopted. And the structural optimization parameters of Energy, Max force and Max displacement were set to be $1.0\times e^{-5}$ Ha, 0.002 Ha/Å and 0.002 Å, respectively. The binding energy (E_b) can be calculated based on the following Equation (1), in which the E_{total} represents the total energy of the coordination polymer, E_{Co} represents the energy of Co ions, and the E_{Ligand} represents the energy of organic ligands connected with the Co centers.

$$E_b = E_{total} - E_{Co} - E_{Ligand} \quad (1)$$

As displayed in Figure 3a, the binding energy of Co-COF with Co coordinated with six O atoms from the adjacent layers of DT-COF structure and two acetate ions (−3.440 eV) is much lower than those for the composite with Co coordinated with six O atoms from COF, one acetate ions and two water molecules (−2.844 eV), as well as the Co composite with only acetate ions and water molecules connection (−1.861 eV). It indicates the stable six coordination mode of Co ions with two O atoms form two COF monomers and other four coordination sites occupied by four O atoms from two acetate ions. It is worth noting that the coordination between Co ions and –NH– units of COF structure is not detected, possibly due to the extremely high binding energy for Co-COF with Co coordinated with –NH– units (Figure S5). Besides, the content of Co in the structure of Co-COF composite has been determined to be 9.37 wt% based on the Inductive Coupled Plasma Emission Spectrometer (ICP) measurements, as shown in Table S1. Furthermore, in order to demonstrate the lithium-ion transfer ability of Co-COF and DT-COF composites, the highest occupied molecular orbital (HOMO) and the lowest unoccupied molecular orbital (LUMO) are calculated based on DFT calculation, as shown in Figure 3b. The HOMO and LUMO of Co-COF have been calculated to be −8.240 eV and −7.212 eV, respectively, forming a band gap of 1.028 eV, which is significantly lower than that of pristine DT-COF (band gap: 2.408 eV). It indicates enhanced Li^+ affinity and low reduction potential for the Co-COF composite, which can be conducive for its rapid ion/electron transfer and resultant enhanced lithium-storage properties.

Adopted as the anode material for lithium-ion battery, the electrochemical properties of Co-COF composite have been evaluated and compared with original DT-COF. As shown in the first three cyclic voltammetric (CV) curves of Co-COF (0.005–3 V; scan rate: 0.1 mV s^{-1}) in Figure 4a, the small wide peak at ~0.62 V and the peaks below 0.50 V in first cathodic scan can be attributed to the formation of an irreversible solid electrolyte interface (SEI) layer at the electrode-electrolyte interface and lithium-ion reaction with the benzene rings from COF structure, respectively.[53] The peak detected at ~1.55 V can be assigned to the reaction between lithium ions and –NH–

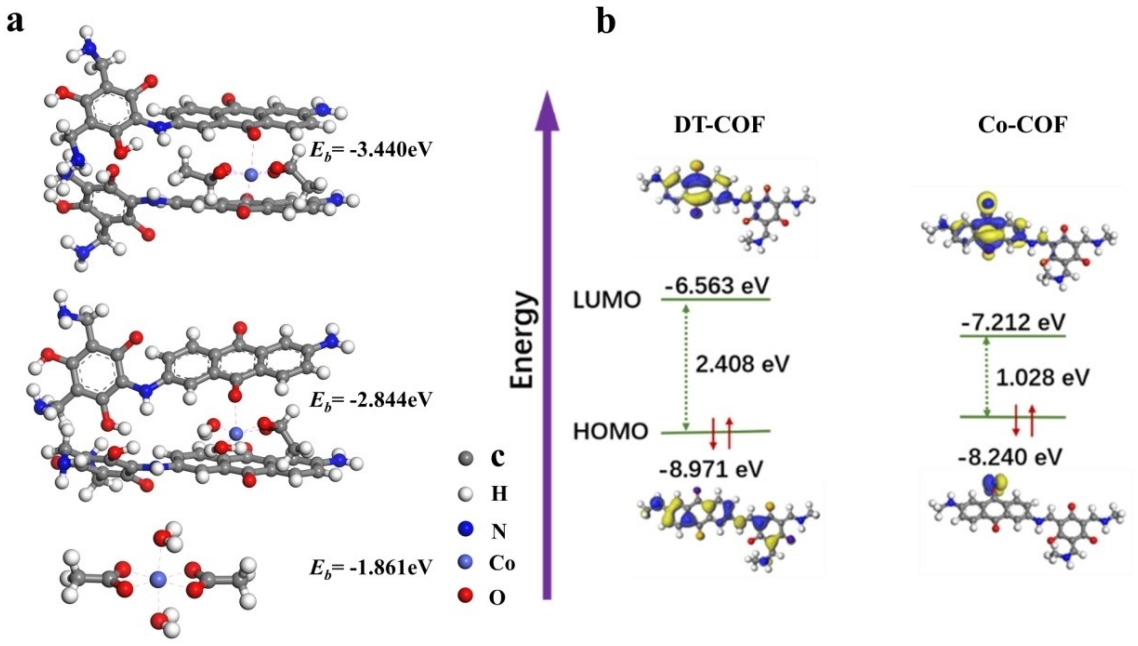

Figure 3. a) Schematic illustration and the binding energy of the Co-COF structure with possible Co coordination environment and the Co composite coordinated with acetate ions. b) Calculated HOMO and LUMO values of DT-COF and Co-COF based on the DFT calculation.

Research Article
doi.org/10.1002/batt.202200434
Chemistry Europe
European Chemical Societies Publishing

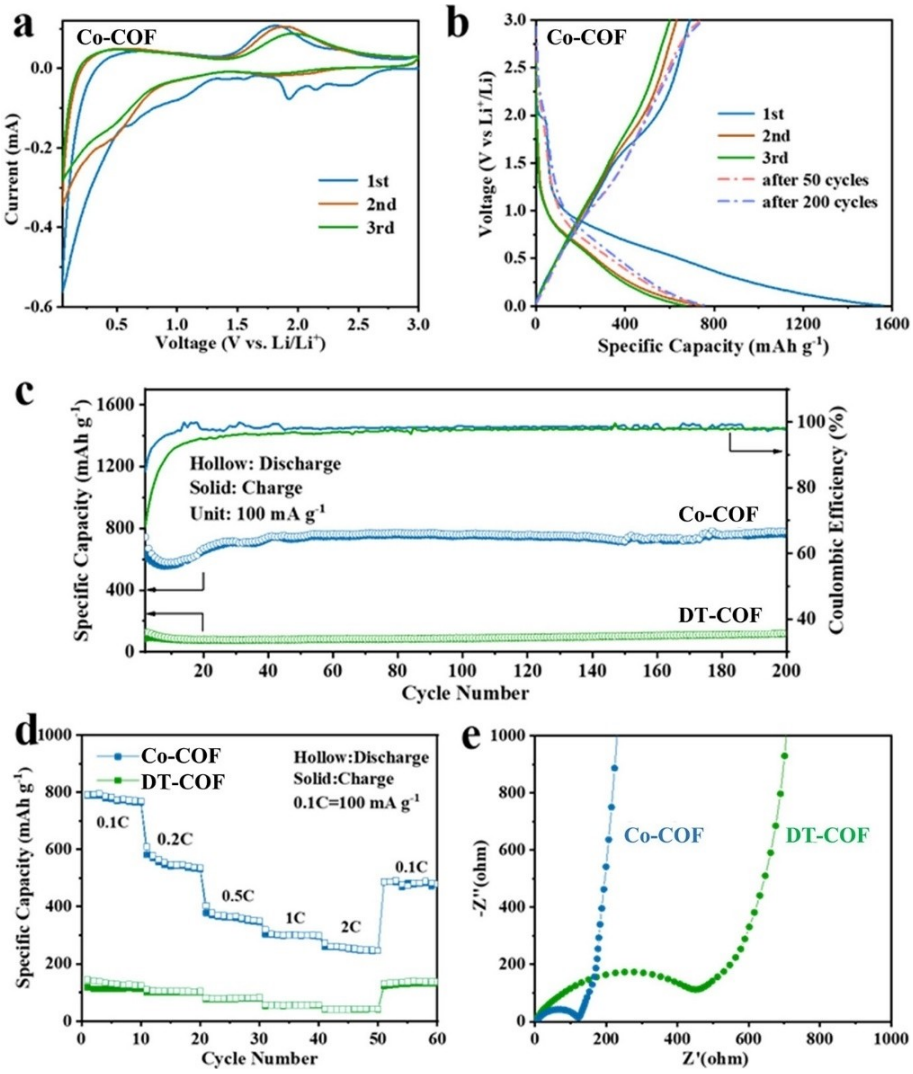

Figure 4. a) Cyclic voltammograms curves and b) charge-discharge curves of Co-COF at 100 mA g^{-1}. c) Cycling performances of Co-COF compared with DT-COF at 100 mA g^{-1}. d) Rate capability of the Co-COF and DT-COF under different current densities. e) Nyquist plots of Co-COF and DT-COF.

groups,[54] which shifts to a higher potential of ~1.80 V in the following two cathodic scan. In the subsequent anodic process, the detected anodic peaks at ~0.40 and 1.80 V indicate the reversible lithium-ion reaction with benzene rings and the –NH– groups. In addition, the reduction peaks at 1.92, 2.10 and 2.40 V correspond to the irreversible embedding of lithium-ions into the C=N and several terminal –NH– groups. The discharge/charge curve of Co-COF (Figure 4b) for the first cycle is basically consistent with its CV results. Initial discharge/charge capacities of Co-COF electrode can be determined to be 1560/698 mAh g^{-1}, with a Coulombic efficiency of 44.37%. The decomposition of electrolyte and the formation of SEI layer result in the significant loss of initial irreversible capacity. After 50 and 100 discharge-charge cycles, the charge capacities of Co-COF electrode increase to 749 and 780 mAh g^{-1}, respectively.

The cyclic performances of the Co-COF and the DT-COF electrodes (Figure 4c) have been evaluated under 100 mA g^{-1}, and the slight capacity decrease can be observed for these two electrodes during the first 10 cycles. Originated from the gradual activation process associated with gradual electrolyte immersion and the activation of functional groups of COF structure, obviously capacity increase during cycling can be detected for the Co-COF electrode after 10 discharge/charge cycles, which reaches 780 mAh g^{-1} after 200 cycles. Comparatively, much lower capacity of 120 mAh g^{-1} can be detected for original DT-COF after the same cycles. In addition, the rate capability of Co-COF and DT-COF was tested under different current rates of 0.1, 0.2, 0.5, 1 and 2 C. As shown in Figure 4d, the Co-COF electrode can achieve a reversible capacity of 296 mAh g^{-1} under current rate of 2 C, and a capacity of 488 mAh g^{-1} can be detected after the current returns to 0.1 C. The decreased capacity compared with the initial value should be ascribed to the partial structural destroy or exfoliation of the Co-COF electrode after charging/discharging under large current densities. Furthermore, as shown in the electrochemical impedance spectroscopy (EIS) results of Co-COF and DT-COF electrodes (Figure 4e), the semicircle in the high frequency

Research Article
doi.org/10.1002/batt.202200434
Chemistry Europe
European Chemical Societies Publishing

region and the diagonal in the low frequency region for each impedance spectrum represent the charge transfer impedance and the Warburg impedance, respectively. Compared with the original DT-COF (R_{ct} = 449.7 Ω), the semicircle diameter of Co-COF is much smaller, indicating the significantly lower calculated charge transfer resistance (R_{ct} = 120.5 Ω) for the Co-COF electrode. It demonstrates that the metal intercalated Co-COF exhibits superior electrochemical conductivity and reaction activity, which can promote the enhanced electrochemical performances of Co-COF electrode, compared with the original DT-COF of this work and previously-reported COF involved electrodes for lithium-storage applications (Table S2).

To further illuminate the structural/functional groups changes during lithium-reaction and the lithium storage mechanism of the Co-COF and DT-COF electrodes, the XPS exploration during their first lithium insertion and extraction process have been conducted (Figure 5). The C 1s spectra for DT-COF and Co-COF can both be divided to five peaks (288.2, 286.8, 285.8, 284.9 and 284.2 eV) corresponding to the C═O, C–O, C–N, C–C and C═C groups.[52] After the lithiation (discharge) process (Figure 5a), a new peak (290.2 eV) corresponding to the C–Li bonds appears in the C 1s spectra for Co-COF electrode, which can be attributed to the lithium-ion reaction with aromatic C═C groups in the benzene ring of COF structure along with the formation of the SEI layer. And during the subsequent delithiation (charge) process, this peak becomes weak rather than disappears, indicating the reversible delithiation reaction on the aromatic C═C groups and the irreversible SEI formation. Besides, the change on the area ratio of peaks assigned to the C–C to C═C groups (increase during the lithiation process and decrease after delithiation) also indicates the lithium-reaction activity of partial aromatic C═C groups in the structure of Co-COF electrode. Furthermore, the peak assigned to the –NH– groups in the N 1s spectra of Co-COF electrode delivers an obvious shift from 399.9 to 400.2 eV with a slight peak-intensity decrease after lithiation and recovers (from 400.2 to 399.9 eV with peak-intensity increase) after subsequent delithiation process (Figure 5c), confirming the reversible lithium-reaction on the –NH– groups. Comparatively, the active aromatic C═C groups and –NH– groups cannot be indicated for the original DT-COF electrode based on its C 1s and N 1s spectra during lithiation and delithiation process,[53–55] as shown in Figure 4b and d. At the same time, no change can be detected for the peaks of Co $2p_{1/2}$, Co $2p_{3/2}$ and their satellite peaks in the Co 2p spectra of Co-COF during lithiation/delithiation process (Figure S6), indicating the inactive Co centers in the Co-COF electrode.

In addition, the *in-situ* FT-IR measurement was also conducted on the Co-COF electrode to further illuminate its lithium-storage mechanism, and the FT-IR spectra during the first discharge/charge (lithiation/delithiation) process between 3.0 V and 0.05 V is shown in Figure 6a. It is observed that the

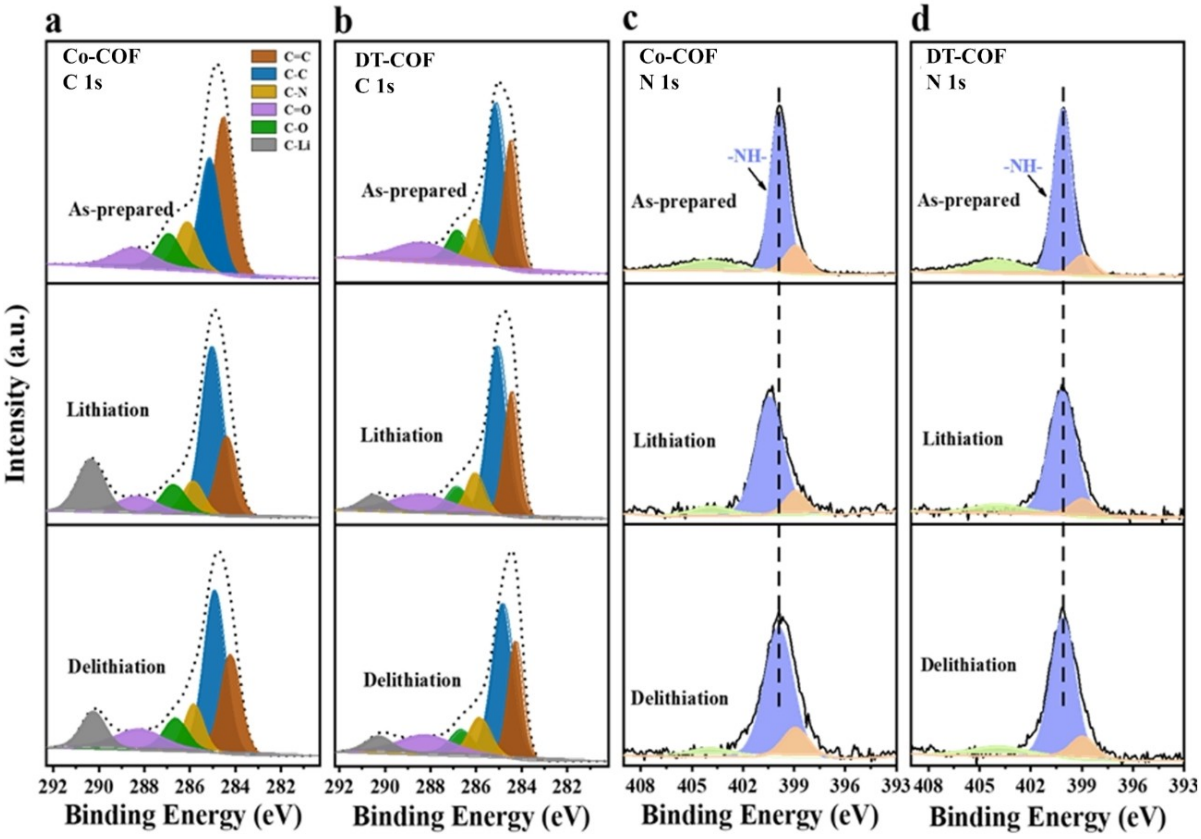

Figure 5. XPS results for the Co-COF and DT-COF electrodes during the first lithiation/delithiation process: a) C 1s scan of Co-COF, b) C 1s scan of DT-COF, c) N 1s scan of Co-COF, d) N 1s scan of DT-COF.

Research Article
doi.org/10.1002/batt.202200434
Chemistry Europe
European Chemical Societies Publishing

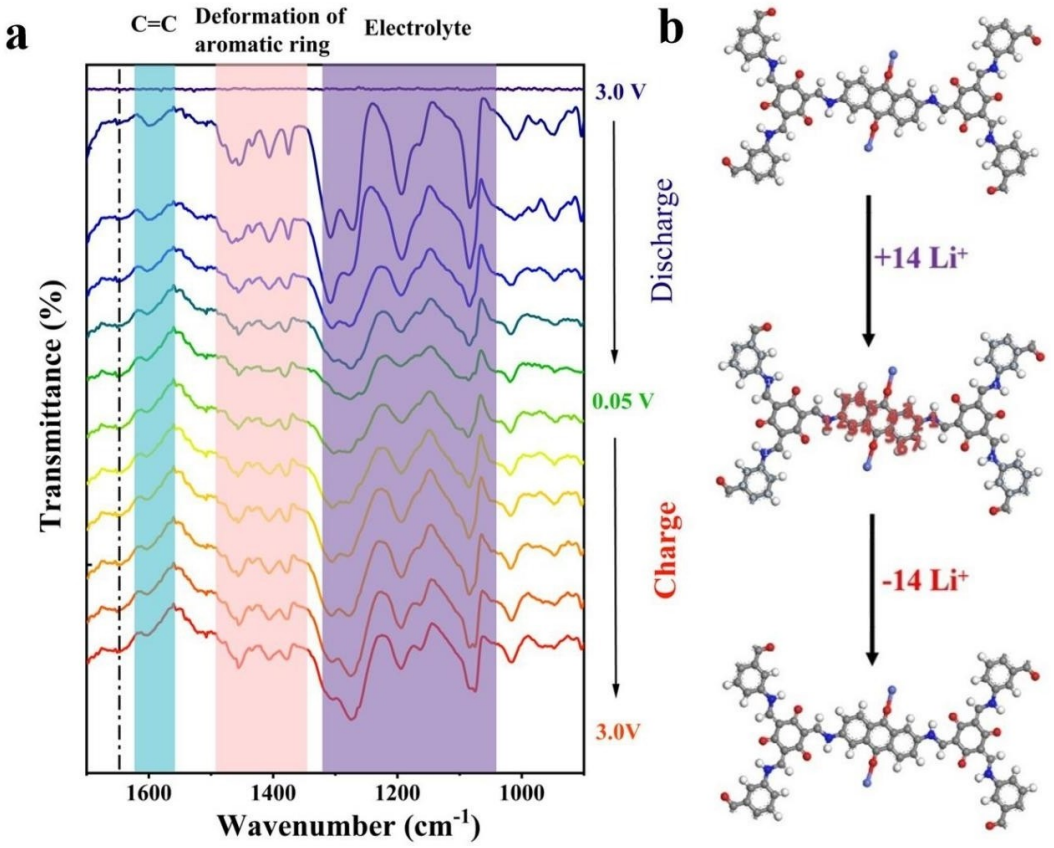

Figure 6. a) *In-situ* FT-IR spectral evolution during the first discharge-charge cycle of Co-COF electrode. b) Proposed schematic illustration of lithium storage in Co-COF structure.

characteristic peak (at around 1581 cm^{-1}) for C=C groups of benzene rings exhibits a weakened trend during the first discharge (lithiation) process (3.0–0.05 V) and the strengthen trend during the following charge (delithiation) process (0.05–3.0 V), indicating the consumption of the C=C groups in the benzene rings for lithium-ion reaction and its reversible lithium-storage activity. However, this peak did not totally return to the original state after complete delithiation, which can be ascribed to the incomplete activation of C=C groups in the Co-COF electrode. The similar change can also be observed for the peaks (1350–1490 cm^{-1}) assigned for the deformation of benzene rings, giving more evidence to the reversible lithium-reaction with benzene rings.[56] The variation on the characteristic peaks in the range of 1050–1310 cm^{-1} should be ascribed to the structural change of the electrolyte during *in-situ* FT-IR measurement. It is worth noting that the peak at around 1646 cm^{-1} assigned to C=O units in the COF structure does not change during the lithiation and delithiation process, indicating the inactive C=O groups for lithium-storage. It can also be confirmed by the unchanged XPS peak for C=O groups during *ex-situ* XPS analysis (Figure 5a and b). The inactive C=O units for lithium-storage is possibly originated from its coordination effects with Co ions.

To further demonstrate the lithium storage mechanism in Co-COF electrode with activated lithium-storage sites, the Generalized Gradient Approximation-Perdew-Burke-Emzerhof (GGA-PBA) functional DFT calculation has been conducted based on the energy and electronic structure of Co-COF. During the calculation, the adopted energy cutoff is 300 eV and the *k*-point set was set to be $1\times1\times6$. During Li-binding process, the speed of the molecule changes from fast to slow and finally stops on the surface of the binding medium. The partial released energy during this process, called binding energy, can be calculated based on the following Equation (2):

$$E_a = \frac{E_0 + nE_{Li^+} - E_T}{n} \quad (2)$$

Among them, E_a represents the average binding energy of Li^+, E_0 represents the total energy of the system before Li^+ is combined, $E_{Li}{}^+$ represents the energy of a single Li^+, E_T represents the total energy of the system after Li^+ is combined, and n is the number of Li^+ combined with the system. As shown in Table 1, the larger average binding energy E_a of Li^+ represents more energy is released during the binding process,

Table 1. The average binding energy of lithium ions on different active sites of DT-COF structure

Site	1	2	3	4	5	6	7
E_a [eV]	1.37	1.00	1.06	1.29	1.20	1.25	0.91

Research Article
doi.org/10.1002/batt.202200434
Chemistry Europe
European Chemical Societies Publishing

and the resultant combined system can be more stable with more lithium-ion combination/storage. The largest average binding energy can be detected for the N position, predicting the preferential lithium reaction on N position. And the binding priority of lithium-reaction on the functional sites in the Co-COF structure can be determined to be the order of 1→4→6→5→3→2→7, as indicated in Figures 6b and S7.

In order to further demonstrate the lithium-storage kinetic behavior of the Co-COF electrode, pseudocapacitance analysis on this electrode has been carried out by CV test under different scanning rates of 0.2–1.0 mV s^{-1}. As shown in Figure 7a, the shape of the CV curves is similar under different scan rates, proving good reversibility of Co-COF electrode. And under the scanning rates of 0.2, 0.4, 0.6, 0.8 and 1.0 mV s^{-1}, the proportions of capacitance contribution can be calculated to be 53.46, 55.47, 57.57, 64.61 and 73.07%, respectively, which is significantly higher than corresponding values for DT-COF electrode (33.25, 42.37, 46.85, 49.84 and 53.17%, respectively) (Figure 7c and d). It indicates the capacitance-dominant behavior of Co-COF electrode and diffusion-controlled behavior of DT-COF electrode. Capacitance-dominant lithium storage behavior endows the Co-COF electrode with fast lithium transfer and reaction, further resulting in its enhanced electrochemical performance. Based on the Galvanostatic Intermittent Titration (GITT) measurements (Figure S8), the lithium diffusion coefficient on the Co-COF electrode can be calculated. Assuming that the transfer of Li^+ satisfies Fick's second law, the diffusion coefficient can be calculated according to the previously reported equation.[55,56] It is indicated that the lithium diffusion coefficient of Co-COF electrode after 200 cycles (1.96×10^{-14}–5.79×10^{-13} $cm^2 s^{-1}$) is obviously higher than that for the electrode after the first cycle (1.80×10^{-15}–1.72×10^{-14} $cm^2 s^{-1}$). It can be attributed to the enhanced kinetics with gradual activation of lithium-reaction functional groups in the Co-COF structure during cycling, and it also leads to the gradually increased reversible capacity of Co-COF electrode.

Conclusion

In summary, we introduce transition metal cobalt intercalated COF as the anode of lithium-ion battery, in which the Co ions were introduced into the synthesis of COF by a facile one-step method. Originated from the coordination-induced Co interca-

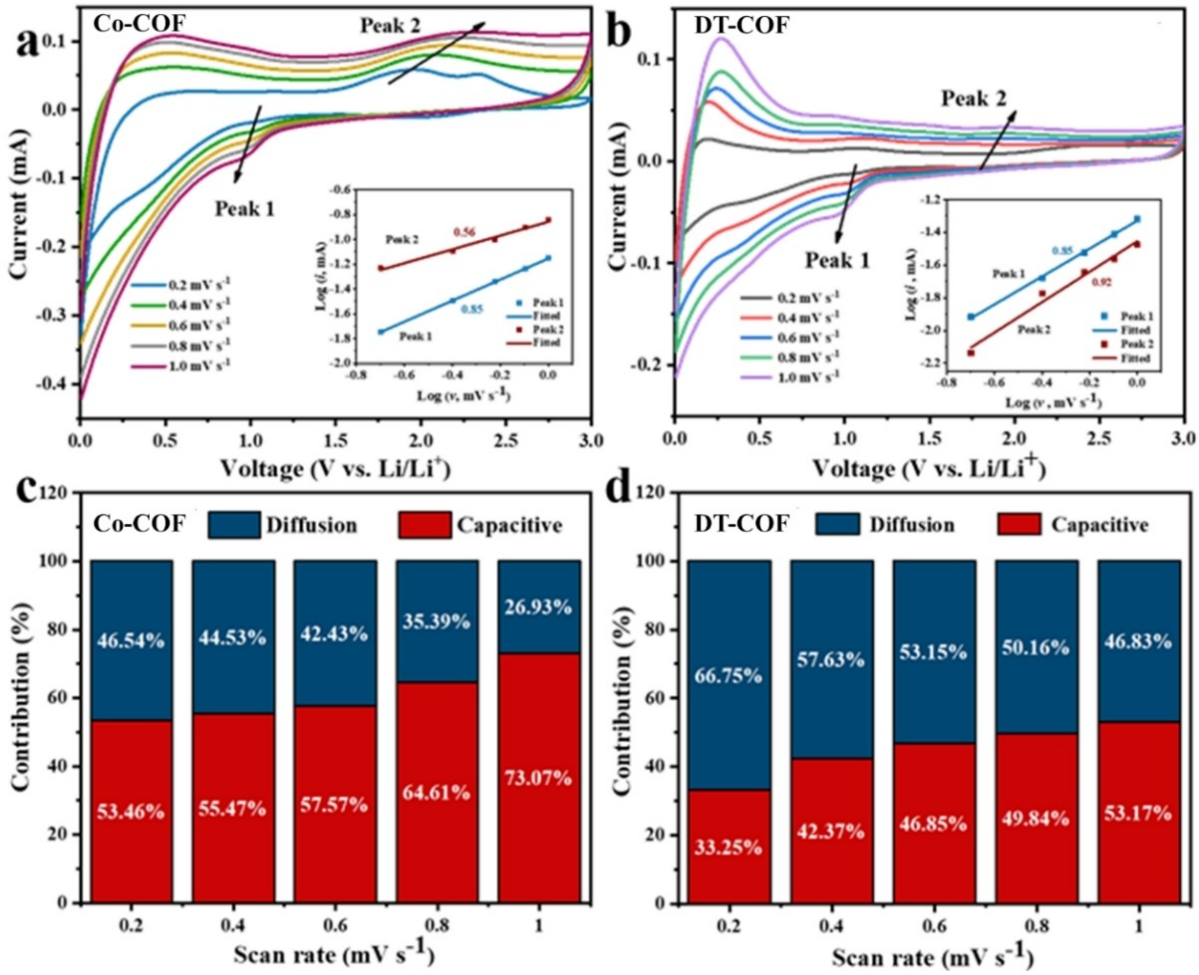

Figure 7. CV profiles of a) Co-COF and b) DT-COF under different scan rates. Insert figure: log(*i*) versus log(*v*) plots. Calculated contribution ratio of capacitive and diffusion-control at scan rate of 0.2–1.0 mV s^{-1} for the c) Co-COF and d) DT-COF electrodes.

lation, the interlayer distance of the original COF can be extended, more functional groups, including C=C of benzene rings and –NH– groups can be activated for lithium storage, and the enhanced Li^+ affinity and low reduction potential with resultant rapid ion/electron transfer can be achieved for the Co-COF electrode. Thus, a large reversible specific capacity of 780 mAh g^{-1} can be detected for the Co-COF electrode compared with 120 mAh g^{-1} of DT-COF at the current density of 100 mA g^{-1} after 200 cycles. In this work, the application of metal intercalated COFs as the organic anode is proposed, which shows the great potential of COFs as electrode materials for high-performance lithium organic battery. And it also provides new ideas for the development of high-capacity organic electrodes for lithium-ion secondary batteries.

Materials and Methods

Materials

2,6-diamino anthraquinone (DAAQ, 97%) was purchased from Aladdin and 1,3,5- triformyl m-triphenol (TFP, 97%) were purchased from J&K Chemicals. 1,4-dioxane (AR, 99%), acetone (AR, 99.5%), dichloromethane (THF, AR, 99%), ethanol (EtOH, AR, 99%) and cobalt acetate tetrahydrate were purchased from Sinopharm Chemical Reagent Co., Ltd. (Shanghai, China). Lithium hexafluorophosphate ($LiPF_6$), polyvinylidene fluoride (PVDF), vinyl carbonate (EC) and diethyl carbonate (DEC) were provided by DoDo Chem. All materials were used directly without further purification.

Synthesis of Co-COF

In a typical process, DAAQ (70 mg), TFP (42 mg), mesitylene/1,4-dioxane were mixed in the Pyrex tube of 10 mL and were stirred for 30 minutes. And then 80 mg $Co(Ac)_2 \cdot 4H_2O$ was added into the mixture above. After stirred for 1 hour, 100 μL 6 M acetic acid was added. The mixture was sonicated for 10 minutes to obtain uniform dispersion. The Pyrex tube was filled with dry nitrogen for 20 minutes and heated to 120 °C for 72 hours. After cooling to room temperature, the precipitate was obtained by centrifugation with acetone/dichloromethane/ethanol. Finally, the brownish red product was obtained by vacuum drying at 60 °C for 12 hours.

Synthesis of DT-COF

DT-COF was synthesized via the similar process as that for Co-COF, without addition of $Co(Ac)_2 \cdot 4H_2O$ and 6 M acetic acid.

Characterization

The size and morphology of the samples were characterized by scanning electron microscope (SEM, JSM-7500F) and transmission electron microscope (TEM, JEOL JEM-200CX). The structure and composition of the materials were analyzed by means of X-ray diffraction (XRD, Rigakud/MAX-2550 V) and Fourier transforms infrared spectroscopy (FTIR, Nicolet 380 FT-IR). High-resolution Solid-state ^{13}C Nuclear Magnetic Resonance (NMR) spectrum, recorded at ambient temperature on an Agilent DSX-300 spectrometer using a standard Agilent magic angle spin (MAS) probe with a 4 mm (outer diameter) zirconia rotor. The X-ray photoelectron spectroscopy (XPS) was carried out on a Thermo Kalpha X-ray photoelectron spectroscopy system. The specific surface area and pore size distribution of the samples were determined by N_2 adsorption using ASAP 2020M + C analyzer. The content of Co in the sample was examined by ICP-MS (Agilent 7700).

Electrochemical tests

The mixed active substances (Co-COF or DT-COF), acetylene black and polyvinylidene fluoride were uniformly mixed according to the mass ratio of 6:3:1 to prepare a negative electrode. The active material loading on copper foil was about 20 μm in thickness of 1.5 mg cm^{-2}. The reference electrode and electrolyte were lithium foil and $LiPF_6$ solution. The lithium foil of the 12 mm disk was the opposite of the reverse electrode used for lithium-ion batteries. Using the LAND CT2001 battery test system at room temperature, the cycle performance and GITT test at different current densities were tested under the potential window of 0.005–3.0 V. The capacity of Co-COF or DT-COF electrodes was calculated according to the total weight of the composites. CV (scanning rate: 0.1–1.0 mV s^{-1}) and EIS (frequency range: 0.01 Hz–100 kHz) were tested on CHI660D electrochemical workstation.

Supporting Information

Supporting Information is available from the Wiley Online Library or from the author.

Acknowledgements

The National Natural Science Foundation of China (52073170), the Innovation Program of Shanghai Municipal Education Commission (2019-01-07-00-09-E00021), Science and Technology Commission of Shanghai (22010500400) and the Innovative research team of high-level local universities in Shanghai are gratefully acknowledged for their financial supports.

Conflict of Interest

The authors declare no conflict of interest.

Data Availability Statement

The data that support the findings of this study are available from the corresponding author upon reasonable request.

Keywords: covalent organic framework · lithium organic batteries · lithium-storage mechanism · organic electrode · metal-ion intercalation

[1] H. Zhang, H. Zhao, M. A. Khan, W. Zou, J. Xu, L. Zhang, J. Zhang, *J. Mater. Chem. A* **2018**, *6*, 20564–20620.
[2] M. Li, J. Lu, Z. Chen, K. Amine, *Adv. Mater.* **2018**, *30*, 1800561.
[3] L. Zhou, K. Zhang, Z. Hu, Z. Tao, L. Mai, Y.-M. Kang, S.-L. Chou, J. Chen, *Adv. Energy Mater.* **2018**, *8*, 1701415.
[4] L. Peng, Y. Zhu, D. Chen, R. S. Ruoff, G. Yu, *Adv. Energy Mater.* **2016**, *6*, 1600025.

[5] H. Kim, W. Choi, J. Yoon, J. H. Um, W. Lee, J. Kim, J. Cabana, W.-S. Yoon, *Chem. Rev.* **2020**, *120*, 6934–6976.
[6] B. Esser, F. Dolhem, M. Becuwe, P. Poizot, A. Vlad, D. Brandell, *J. Power Sources* **2021**, *482*, 228814.
[7] P. Poizot, J. Gaubicher, S. Renault, L. Dubois, Y. Liang, Y. Yao, *Chem. Rev.* **2020**, *120*, 6490–6557.
[8] X. Cui, H. Dong, S. Chen, M. Wu, Y. Wang, *Batteries & Supercaps* **2021**, *4*, 72–97.
[9] Y. Hara, K. Sakaushi, *Nanoscale* **2021**, *13*, 6341–6356.
[10] R. Rojaee, R. Shahbazian-Yassar, *ACS Nano* **2020**, *14*, 2628–2658.
[11] Y. Cao, W. Sun, C. Guo, L. Zheng, M. Yao, Y. Wang, *ACS Nano* **2022**, *16*, 9830–9842.
[12] R. C. K. Reddy, X. Lin, A. Zeb, C.-Y. Su, *Electrochem. Energy Rev.* **2022**, *5*, 312–347.
[13] A. K. Thakur, M. Majumder, S. P. Patole, K. Zaghib, M. V. Reddy, *Adv. Mater.* **2021**, *2*, 2457–2482.
[14] K. Geng, T. He, R. Liu, S. Dalapati, K. T. Tan, Z. Li, S. Tao, Y. Gong, Q. Jiang, D. Jiang, *Chem. Rev.* **2020**, *120*, 8814–8933.
[15] T. F. Machado, M. E. S. Serra, D. Murtinho, A. J. M. Valente, M. Naushad, *Polymer* **2021**, *13*, 970.
[16] J. You, Y. Zhao, L. Wang, W. Bao, *J. Cleaner Prod.* **2021**, *291*, 125822.
[17] Q. Yang, M. Luo, K. Liu, H. Cao, H. Yan, *Appl. Catal. B.* **2020**, *276*, 119174.
[18] N. Kundu, S. Sarkar, *J. Environ. Chem. Eng.* **2021**, *9*, 105090.
[19] Z. Wang, W. Jin, X. Huang, G. Lu, Y. Li, *Chem. Rev.* **2020**, *20*, 1198–1219.
[20] X. Zhao, P. Pachfule, A. Thomas, *Chem. Soc. Rev.* **2021**, *50*, 6871–6913.
[21] V. Singh, H. R. Byon, *Adv. Mater.* **2021**, *2*, 3188–3212.
[22] D.-G. Wang, T. Qiu, W. Guo, Z. Liang, H. Tabassum, D. Xia, R. Zou, *Energy Environ. Sci.* **2021**, *14*, 688–728.
[23] Q. Geng, H. Wang, J. Wang, J. Hong, W. Sun, Y. Wu, Y. Wang, *Small Methods* **2022**, *6*, e2200314.
[24] C. Guo, J. Yang, Z. Cui, S. Qi, Q. Peng, W. Sun, L.-P. Lv, Y. Xu, Y. Wang, *J. Energy Chem.* **2022**, *65*, 514–523.
[25] S.-Q. Li, L. Zhang, T.-T. Liu, Y.-W. Zhang, C. Guo, Y. Wang, F.-H. Du, *Adv. Mater.* **2022**, *34*, 2201801.
[26] R. Freund, O. Zaremba, G. Arnauts, R. Ameloot, G. Skorupskii, M. Dincă, A. Bavykina, J. Gascon, A. Ejsmont, J. Goscianska, M. Kalmutzki, U. Lächelt, E. Ploetz, C. S. Diercks, S. Wuttke, *Angew. Chem. Int. Ed.* **2021**, *60*, 23975–24001; *Angew. Chem.* **2021**, *133*, 24174–24202.
[27] T. Liu, J. Hong, J. Wang, Y. Xu, Y. Wang, *Energy Storage Mater.* **2022**, *45*, 1074–1083.
[28] D. Xu, M. Liang, S. Qi, W. Sun, L.-P. Lv, F.-H. Du, B. Wang, S. Chen, Y. Wang, Y. Yu, *ACS Nano* **2021**, *15*, 47–80.
[29] J. J. Shea, C. Luo, *ACS Appl. Mater. Interfaces* **2020**, *12*, 5361–5380.
[30] S.-m. Zeng, X.-x. Huang, Y.-j. Ma, L.-j. Zhi, *New. Carbon. Mater.* **2021**, *36*, 1–18.
[31] T. Sun, J. Xie, W. Guo, D.-S. Li, Q. Zhang, *Adv. Energy Mater.* **2020**, *10*, 1904199.
[32] G. Zhao, Y. Zhang, Z. Gao, H. Li, S. Liu, S. Cai, X. Yang, H. Guo, X. Sun, *ACS Energy Lett.* **2020**, *5*, 1022–1031.
[33] E. R. Wolfson, N. Xiao, L. Schkeryantz, W. K. Haug, Y. Wu, P. L. McGrier, *Mol. Syst. Des. Eng.* **2020**, *5*, 97–101.
[34] Y. Tong, X. Wang, Y. Zhang, W. Huang, *Inorg. Chem. Front.* **2021**, *8*, 558–571.
[35] G. Zhao, Z. Mei, L. Duan, Q. An, Y. Yang, C. Zhang, X. Tan, H. Guo, *Carbon Energy* **2022**, 1–13.
[36] G. Zhao, H. Li, Z. Gao, L. Xu, Z. Mei, S. Cai, T. Liu, X. Yang, H. Guo, X. Sun, *Adv. Funct. Mater.* **2021**, *31*, 2101019.
[37] J. Wang, N. Li, Y. Xu, H. Pang, *Chem. Eur. J.* **2020**, *26*, 6402–6422.
[38] Y. Tao, W. Ji, X. Ding, B.-H. Han, *J. Mater. Chem. A* **2021**, *9*, 7336–7365.
[39] S. Ruan, D. Luo, M. Li, J. Wang, L. Ling, A. Yu, Z. Chen, *Energy Storage Mater.* **2021**, *38*, 200–230.
[40] Y. Hu, L. J. Wayment, C. Haslam, X. Yang, S.-h. Lee, Y. Jin, W. Zhang, *EnergyChem* **2021**, *3*, 100048.
[41] H. Chen, Q.-H. Li, W. Yan, Z.-G. Gu, J. Zhang, *Chem. Eng. J.* **2020**, *401*, 126149.
[42] J. Liu, T. Cheng, L. Jiang, H. Zhang, Y. Shan, A. Kong, *Electrochim. Acta* **2020**, *363*, 137280.
[43] S. Wang, Y. Liang, T. Dai, Y. Liu, Z. Sui, X. Tian, Q. Chen, *J. Colloid Interface Sci.* **2021**, *591*, 264–272.
[44] B. Han, X. Ding, B. Yu, H. Wu, W. Zhou, W. Liu, C. Wei, B. Chen, D. Qi, H. Wang, K. Wang, Y. Chen, B. Chen, J. Jiang, *J. Am. Chem. Soc.* **2021**, *143*, 7104–7113.
[45] D. Song, H. Guo, K. Huang, H. Zhang, J. Chen, L. Wang, C. Lian, Y. Wang, *Mater. Today* **2022**, *54*, 42–51.
[46] Q. Li, X. Lan, G. An, L. Ricardez-Sandoval, Z. Wang, G. Bai, *ACS Catal.* **2020**, *10*, 6664–6675.
[47] L. Zhao, L. Zheng, X. Li, H. Wang, L.-P. Lv, S. Chen, W. Sun, Y. Wang, *ACS Appl. Mater. Interfaces* **2021**, *13*, 48913–48922.
[48] C. R. DeBlase, K. E. Silberstein, T.-T. Truong, H. D. Abruña, W. R. Dichtel, *J. Am. Chem. Soc.* **2013**, *135*, 16821–16824.
[49] E. Vitaku, C. N. Gannett, K. L. Carpenter, L. Shen, H. D. Abruña, W. R. Dichtel, *J. Am. Chem. Soc.* **2020**, *142*, 16–20.
[50] X. Kong, S. Zhou, M. Strømme, C. Xu, *Carbon* **2021**, *171*, 248–256.
[51] M. Lu, Q. Li, J. Liu, F.-M. Zhang, L. Zhang, J.-L. Wang, Z.-H. Kang, Y.-Q. Lan, *Appl. Catal. B* **2019**, *254*, 624–633.
[52] Z. Lei, Q. Yang, Y. Xu, S. Guo, W. Sun, H. Liu, L.-P. Lv, Y. Zhang, Y. Wang, *Nat. Commun.* **2018**, *9*, 576.
[53] X. Chen, Y. Li, L. Wang, Y. Xu, A. Nie, Q. Li, F. Wu, W. Sun, X. Zhang, R. Vajtai, P. M. Ajayan, L. Chen, Y. Wang, *Adv. Mater.* **2019**, *31*, 1901640.
[54] Z. Lei, X. Chen, W. Sun, Y. Zhang, Y. Wang, *Adv. Energy Mater.* **2019**, *9*, 1801010.
[55] J. Wu, X. Rui, G. Long, W. Chen, Q. Yan, Q. Zhang, *Angew. Chem. Int. Ed.* **2015**, *54*, 7354–7358; *Angew. Chem.* **2015**, *127*, 7462–7466.
[56] X. Tang, Y. Zhang, W. Sun, Y. Wang, *ACS Appl. Energ. Mater.* **2020**, *3*, 11378–11387.

Manuscript received: September 30, 2022
Revised manuscript received: December 12, 2022
Accepted manuscript online: December 26, 2022
Version of record online: January 13, 2023